JMEPEG
https://doi.org/10.1007/s11665-020-05198-7

1059-9495/$19.00

Different Cr Contents on the Microstructure and Tribomechanical Properties of Multi-Layered Diamond-Like Carbon Films Prepared by Unbalanced Magnetron Sputtering

Li-na Zhu, Jun-chao Li, Jia-jie Kang, Ling Tang, Guo-zheng Ma, Cui-hong Han, Jia-dong Shi, and Hai-dou Wang

(Submitted March 4, 2020; in revised form August 31, 2020; Accepted September 19, 2020)

To investigate the effects of Cr doping on the microstructure and tribological properties of multi-layered diamond-like carbon (DLC) films, Cr-DLC films with Cr contents ranging from 0 to 22 at.% were deposited on 0Cr19Ni10 stainless steel and Si wafer surfaces by unbalanced magnetron sputtering. The thickness of the transition layer is 180 nm and the Cr-DLC film ranging from 1.3 to 1.5 µm. The microstructure, mechanical and tribological properties of the films were systematically investigated at room temperature in atmospheric environment. Results show that increasing the Cr target current can effectively improve the incident particle density and reduce surface roughness. As a strong carbon metal, Cr has significant influence on the structure and properties of the film for bonding with carbon atoms during deposition. High-energy Cr particles are favorable for films to increase the sp^3 hybrid bond ratio and reduce internal stress. The high-hardness sp^3 hybrid phase, Cr carbide, oxide dispersion can effectively improve the mechanical properties of the film, but overdoping is detrimental for mechanical properties of the film. The internal stress shows a continuous trend of decreasing with the increasing Cr content and it reduced up to 80% compared with pure DLC films. The films prepared with Cr sputtering current of 0.4 A demonstrate the best tribological properties, and the friction coefficient and wear rate are 0.15 and 2.9×10^{-7} mm^3/Nm, respectively.

Keywords DLC films, doping, mechanical properties, tribological behaviors

1. Introduction

Carbon materials play a vital role in human development because of their diverse nature, such as electromagnetic properties, thermal properties, optical properties, and microelectronics (Ref 1, 2). They are known as one of the most viable materials in twenty-first century. Among the new carbon materials, diamond-like carbon (DLC) films are widely used in aerospace, machinery and biology because they contain sp^3 hybrid carbon atoms of diamond structure and sp^2 hybrid carbon atoms of graphite structure (Ref 3). So, DLC exhibits an extremely good performance of diamond and graphite simultaneously (Ref 4, 5). Physical vapor deposition and chemical vapor deposition are two common techniques for preparing DLC films (Ref 6, 7). Modification of the structure and composition of the film can be accomplished by using a transition layer (Ref 8, 9), a multilayer layer (Ref 10, 11), and doping (Ref 12, 13), which are not only important methods to improve the overall performance of the film, but also meaningful for engineering applications. In the above methods, doping has the most significant influence on the structure and properties of the DLC films, especially doping of transition metals (Ref 14-17).

Research shows metals with strong binding capacity to carbon, such as Cr, W, Mo, and others can easily form hard metal carbides and oxides in the film (Ref 10, 18-21). In addition, there are many unbound atoms, such as elemental Cr or single metals, which are nonuniformly distributed in the three-dimensional network structure of amorphous carbon to form a multi-component composite structure of nanocrystals and amorphous states. The mechanical properties of the film can be enhanced by the dispersion strengthening of multiphase particles. In the process of bonding with carbon atoms, the doping atoms break the combination of the original hybrid carbon atoms, which leads to the relative content of sp^2 and sp^3 hybrid bonds in the film are affected greatly, so the overall performance of the film has been dramatically changed. It is generally accepted that the π bond in the sp^2 hybrid form determines the photoelectric properties and self-lubricity of the film, while the σ bond in the sp^3 hybrid form determines the mechanical properties of the film (Ref 22-25). The properties of the film vary greatly under different ratios of these hybrid types, and there are several orders of magnitude of difference among

Li-na Zhu and **Jia-jie Kang**, School of Engineering and Technology, China University of Geosciences (Beijing), Beijing 100083, China; and Zhengzhou Institute, China University of Geosciences (Beijing), Zhengzhou 451283, China; **Jun-chao Li, Ling Tang, Guo-zheng Ma,** and **Hai-dou Wang**, School of Engineering and Technology, China University of Geosciences (Beijing), Beijing 100083, China; and National Key Laboratory for Remanufacturing, Army Academy of Armored Forces, Beijing 100072, China; and **Cui-hong Han** and **Jia-dong Shi**, National Key Laboratory for Remanufacturing, Army Academy of Armored Forces, Beijing 100072, China; and School of Materials Science and Engineering, Hebei University of Technology, Tianjin 300130, China. Contact e-mail: magz0929@163.com.

Published online: 23 October 2020

the resistivity, friction coefficient, and hardness of these materials. The metals with weak binding capacity to carbon, such as Cu, Ag, Au (Ref 11, 26-31), have valence electron orbitals in their full state, and they hardly react with carbon atoms. These materials mainly form nanocrystals distributed in carbon structure network. High-speed and high-energy particles which bombard the substrate produce large internal stress during the deposition process, yet the nanocrystals can reduce this internal stress effectively and improve the toughness of the films. Moreover, high chemical reactivity of the nanocrystals can be combined with oxygen atoms to form a passivation film on the surface, preventing oxidation from atomic oxygen effectively, and it is also a good self-lubricating material for its low shear strength (Ref 32). Tribological properties, as one of the most important properties of DLC films, have attracted wide attention after being reported for the first time due to their low friction coefficient and high hardness. The adsorption and passivation effect of surface dangling bonds on heterogeneous atoms can effectively reduce the friction coefficient. The DLC films prepared by vapor deposition have a lower surface roughness than other preparation technologies, which can effectively reduce the running-in phase during the rubbing process. Cr-doped DLC films exhibit attractive tribological performance compared with undoped DLC films due to their low stress, thermal stability and bond strength (Ref 33-35). Most of them demonstrate ideal properties with increasing of Cr content. However, the influence of over-doping and mechanism of doping on the structural properties of DLC films need to be revealed.

In order to further investigate the influence of doping on the structural properties of DLC films, unbalanced magnetron sputtering was used to dope Cr in DLC films in this study. The influence of Cr doping on the microstructure, composition, mechanical properties, and tribological properties of the films was analyzed and the mechanism was revealed.

2. Materials and Methods

2.1 Films Preparation

Transition layer, DLC films, and Cr doping DLC films were deposited by unbalanced magnetron sputtering. There are three rectangular sputtering targets and one ion source deposition equipment. In this study, a pure graphite target was installed on the No. 1 target, a pure chromium target was installed on the No. 3 target, and the No. 2 target was not used. In order to characterize the structure and properties of the film, 0Cr19Ni10 ($20 \times 30 \times 5$ mm) stainless steel and silicon (111) wafers (Φ 50×0.3, Ra $\leq$ 2 nm) were selected as the substrates for wear test and microstructure characterization, respectively.

The substrates are ultrasonically cleaned in deionized water for 10 min, alcohol for 10 min, and acetone for 10 min, successively. Then, they were dried and placed in vacuum chamber and the chamber was pumped down to 6×10^{-3} Pa. In order to improve the adhesion between the film and the substrate, the substrate was subjected to Ar ion cleaning for 20 min before deposition to improve the interfacial activity of the substrate, which can increase the bonding strength between the transition layer and substrate. The chromium target was sputtered before depositing the DLC film. The deposition time was 10 min to form the first stress buffer layer of Cr. Then, to form the second buffer layer of Cr and C, the sputtering current of Cr target increased 0.02 A per minute and the total deposition time is 10 min. Finally, the work layer was deposited, with the deposition parameters of the specific working layer were shown in Table 1. When the Cr target current was at 0 A, the corresponding thin structure was assigned as the substrate/Cr/CrC/DLC, and when the Cr target current was 0.2, 0.4 and 0.6 A, the corresponding film structure was assigned to substrate/Cr/CrC/Cr-DLC, recorded as DLC, Cr-0.2, Cr-0.4, Cr-0.8.

2.2 Characterization of the Films

A ZEISS Supra55 field-emission scanning electron microscope was used to observe the cross section and surface morphology of the films. The roughness, hardness, and elastic modulus of the films were tested by a comprehensive mechanical performance tester (Hysitron TriboScope, Bruker, Germany) with an atomic force microscope and a nanoindenter. Using the same probe and testing for nanoindenter experiments first. The maximum load was 1000 μN and the depth of the nanoindentation ranged from 80 to 100 nm. The loading time, holding time, and unloading time were 5 s. Then the probe was scanned on the surface to measure the surface roughness with a scan range of 20 μm. The compressive residual stress was measured by D-500 Stylus Profiler of KLA-Tencor, A self-developed MSTS-1 multi-functional ball-disk friction and wear tester were used to test the tribological performance of the films in the atmosphere. In this work, the upper samples were 9Cr18 stainless steel balls with diameter of 9.525 mm, and the applied load was 6 N, the rotation speed was 300 r/min, and the rotation radius was 5 mm, the friction time was 20 min (Ref 31). After the friction and wear tests, an Olympus-OLS4000 three-dimensional shape analyzer (Olympus OLS4000, Japan) was used to observe the wear scar morphology and calculate the wear rate (Ref 36). The film was subjected to Raman spectroscopy using a Renishaw in Via plus laser Raman spectrometer (HR-800, HORIBA JobinYvon, France, wavelength = 633 nm) to analyze the bond structure characteristics. The elemental composition and chemical valence state of the films were analyzed by XPS (ESCALAB 250Xi, Thermo Scientific), and etching is performed for 2 min before the test to remove the effects of surface impurities and oxidation.

Table 1 Parameters for film deposition

Parameter	Value
Work pressure, Pa	5.1
Ar, sccm	60
Substrate bias voltage, V	− 50
Substrate temperature, °C	200
C sputtering current, A	4.8
Cr sputtering current, A	0, 0.2, 0.4, 0.8
Cr/CrC interlayer deposition time, min	20
DLC deposition time, min	240

3. Results and Discussion

3.1 Microstructure and Composition

The surface and cross section of the four samples were observed using a scanning electron microscope. As shown in Fig. 1, the transition layers were all 180 nm. As the Cr target current increased, the thickness of the film did not increase significantly, ranging from 1.3 to 1.5 μm, because high current represents a high deposition rate. It can be seen from the cross section that upon turning off Cr target, as shown in Fig. 1(a2), the material appears as a pure, diamond-like film, which is a kind of amorphous carbon-based film and its structure is a three-dimensional network with short-range order and long-range disorder. It means that there are no large-sized columnar crystals from on surface, and only the localized small regions appear in an ordered arrangement, existing in ordered structural domains that are not constrained from each other. Figure 1(b2, c2, d2) shows the cross-sectional morphology of the Cr target currents of 0.2, 0.4 and 0.8 A, respectively. A columnar crystal structure with a clear penetrability can be observed because Cr is a simple substance, and Cr compounds have typical crystal structures that affect the overall structure of the film. It can be seen that a discontinuous structure occurs in a localized region due to film breakage. Comparing c2 and d2, the columnar crystal is tiny, because with the increase in the current of the Cr target, particles have higher sputtering energy and kinetic energy, so it is easier to enter the gap of the carbon structure network and make the structure dense.

The morphologies of the films are displayed in Fig. 1(a1, b1, c1, d1), the amorphous carbon-based film is black-gray, and the film changed from black gray to white gray as the Cr target current increased, results show that the Cr content in the film increased constantly. The surface of the four films exhibited nanoscale, cluster-like and granular structure. The surface roughness of the film was tested by atomic force microscopy, as shown in Fig. 2. When the Cr target current was 0.2 A, crystal particles appeared on the surface that were not present on the pure DLC film, a randomly grown and uneven distribution of protrusions can be seen, and the surface roughness increased from 4.6445 nm (pure DLC film) to 4.879 nm. With the increasing of Cr target current, the roughness showed a downward trend, from 4.879 nm at 0.2 A to 3.846 nm at 0.8 A, because the increasing of target current can effectively increases the energy and density of the sputtered particles in the coating chamber, more particles deposited on the surface per unit time and the columnar structure become more compact. The C and Cr compounds were uniformly distributed in the three-dimensional network of the film, making the surface more smoother and denser.

Raman plays an important role in diamond characterization (Ref 37-39). Figure 3 shows the Raman spectra of DLC films deposited under different Cr target currents. The spectra of the four samples range from 1000 to 1800 cm^{-1} and show asymmetric, broad peaks. The pure DLC film (red line) peak is obtained by Gaussian fitting. The curve is decomposed into a D peak near 1386 cm^{-1} and a G peak near 1581 cm^{-1}, which are typical diamond-like peaks. With the increase of Cr target current, the Cr content in the film increases continuously, and the intensities of the G and D peaks decrease, indicating that Cr doping reduces the order of the structure. Besides, the introduction of extraneous high-energy particles is distributed in the carbon structure network, increasing the number of interstitial atoms. The dotted line in Fig. 3(b) is the line connecting the D and G peaks after the four peaks are fitted. As the Cr content increases, both G and D peaks move toward lower wavenumbers, which also indicates the disorder of bond angles increases continuously, and the degree of short-range order decreases. The left shift of the D peak represents that there is an increase in the number of coordination carbon atoms, the content of sp^2 hybrid bonds in the film decreases, and the content of graphite phase decreases (Ref 40, 41).

Figure 4 shows the I_D/I_G value and G peak positions of the four samples. In the amorphous carbon films, the relative intensity ratio of I_D/I_G of the D and G peaks is inversely proportional to the grain size, indicating that as the content of Cr increases, the value of I_D/I_G decreases, and the grain size continues to increase (Ref 11). It is generally accepted that the D peak represents sp^2 hybrid carbons that form graphite rings, and I_D/I_G can be used as a parameter to estimate the content of sp^3 hybrid bonds. The smaller the ratio, the higher the content of sp^3 hybrid bond. The microstructure of the film is very sensitive to Cr metal doping. As the Cr target current increases

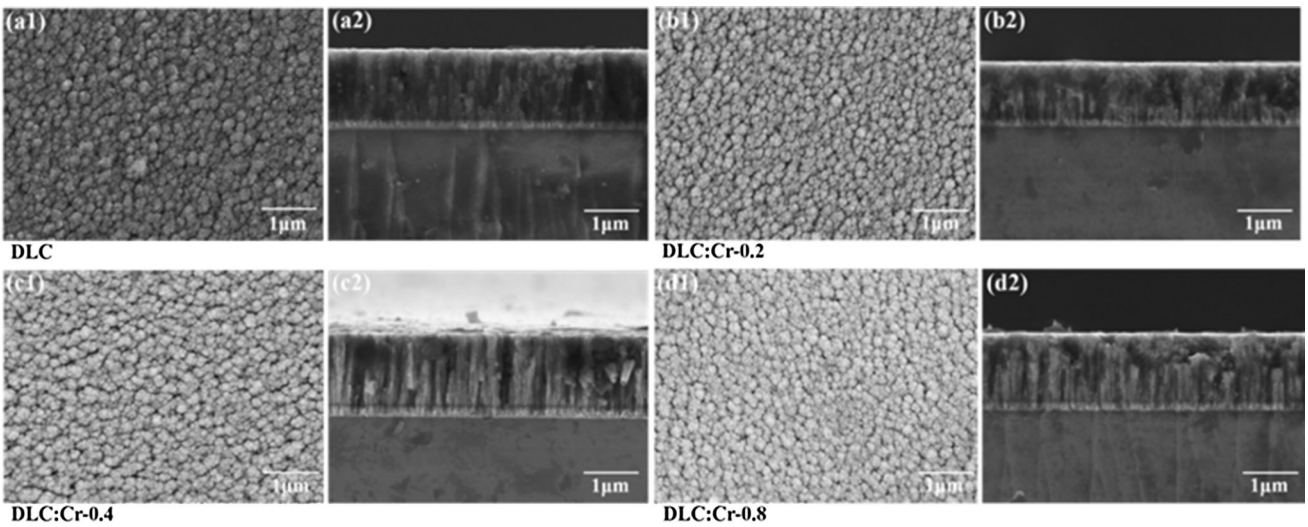

Fig. 1 SEM surface and cross-sectional images of (a1, a2) DLC, (b1, b2) Cr-0.2, (c1, c2) Cr-0.4, (d1, d2) Cr-0.8

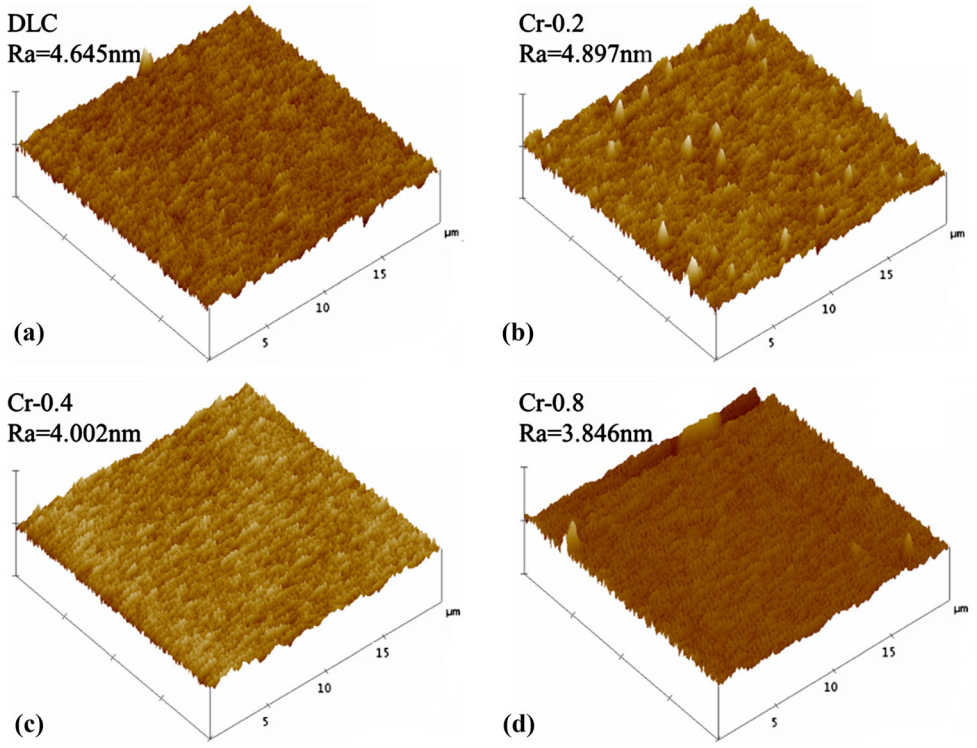

Fig. 2 3D images and roughness of (a) DLC, (b) Cr-0.2, (c) Cr-0.4, and (d) Cr-0.8 films

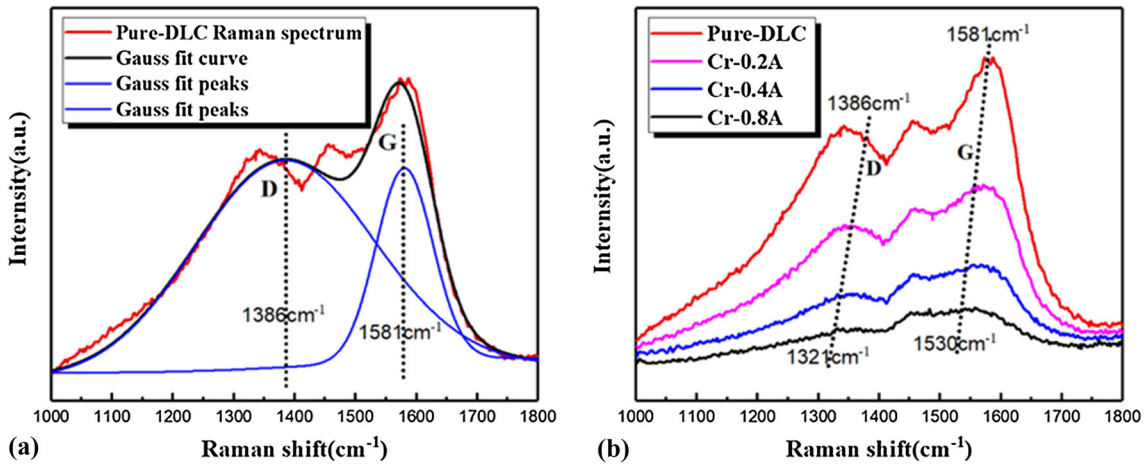

Fig. 3 Typical Raman spectra of (a) DLC and (b) Cr-DLC films

from 0 to 0.8 A, the proportion of sp^3 hybrid bonds in the film increases. Because the density and energy of the incident particles increased with the sputtering target current. During the collision deposition process, the nucleation process and the growth process are both limited by space. The newly deposited particles do not migrate or completely migrate before nucleation. The extrusion of the new incident particle is restricted in movement, causing the stress to not to be released and be in a bound state, which increases the internal stress. During the film deposition process, the internal stress determines the sp^3 hybrid phase. In other words, stress determines the content of the diamond phase. The high incident energy and impact velocity can significantly increase the level of stress on the surface of the substrate, and the diamond phase content increases significantly. At the same time, the formation of sp^3 hybrid bonds in the film also moves with the G peak to lower wavenumbers, and the content of sp^2 hybrid bonds decreases. This indicates that the content of the three-dimensional network structure in the film increases, the content of the graphite ring structure decreases, and the carbon atoms tend to become of a higher coordination binding nature.

Qualitative and quantitative analyses of elements in the film are usually performed by XPS. Figure 5 shows (a) full spectrum, (b) C1s, (c) O1s, and (d) Cr2p spectra of XPS after etching. While the Cr target current increases from 0.2 to 0.4 to 0.8 A, the Cr atom concentration of film increases from 5 to 11 at.% to 22 at.%, respectively. The doping of Cr atoms directly affects the short-range order of the carbon structure, the relative intensity of the C1*s* peak decreases, and the atomic concentration decreases. At the same time, the concentration of

oxygen atoms increases with the increase of Cr content, rising from 1.12 to 4.77 at.%. It can be seen from Fig. 5(b) that oxygen is mainly present in the film in the form of carbon–oxygen bonds before doping. Due to the large concentration of high-speed, sputtered particles, some of the carbon oxides have no time to diffuse and form tiny gaseous masses, fixing to the carbon structure network of the film at a relatively small content. When Cr atom is doped, it can be concluded from Fig. 5(c) that the form of O element changed from the C-O to the Cr-O bond and mostly occurs with metal oxide in the network structure. The Cr can be found in Fig. 5(d), compared with elemental C and O, has larger difference in electronegativity. During the deposition process, the O atom preferentially combines with the Cr atom. The larger the incident current, the higher energy the Cr particle, Cr atoms are easy to break through the energy barrier and produce a chemical reaction, causing the content of oxygen atom to increase.

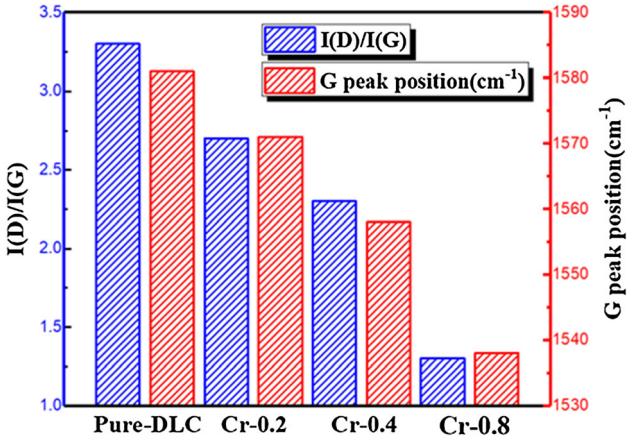

Fig. 4 I_D/I_G and G peak position of the DLC, Cr-0.2, Cr-0.4, and Cr-0.8 films

It can be seen from Fig. 5(d) that the Cr is mainly present in the forms of metal and metal carbide in the film. The part of Cr is completely bombarded on the surface with the form of single atoms, and others become small atomic clusters. The single Cr atoms and outside surface atoms of these small groups that are sputtered bond with O atoms or C atoms to form compounds during flight or as they reach the surface, but at the center of the cluster, the atom fails to come in contact with other atoms or they reach the surface of the substrate, which still maintains the

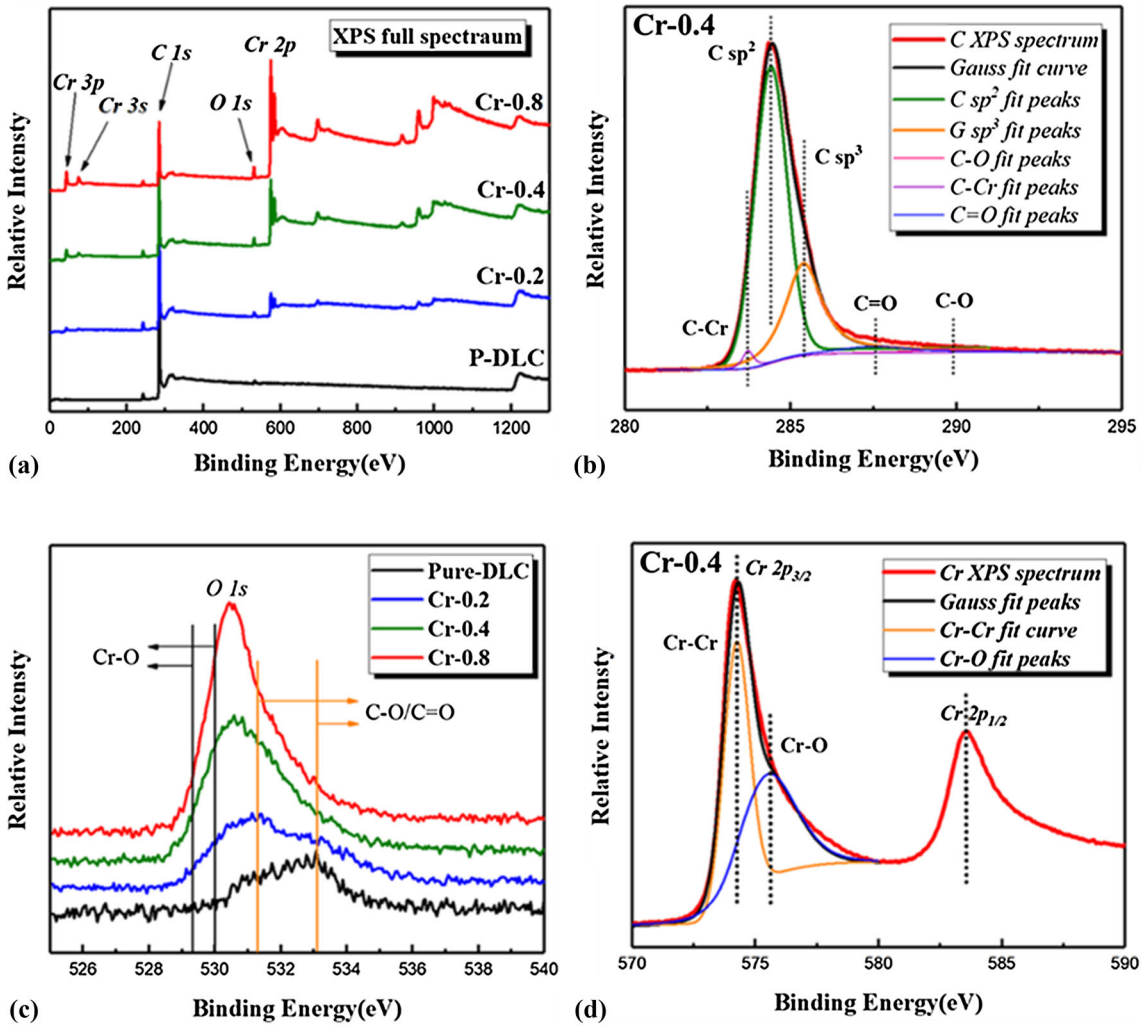

Fig. 5 The XPS spectra of (a) full spectrum, (b) C1s spectrum with Cr-0.4, (c) O1s spectrum, and (d) Cr2p spectrum with Cr-0.4

Cr-Cr metal bond. The bonding energy in the Cr spectrum is 577.4 and 574.4 eV, representing two combinations of Cr.

Figure 6(a) illustrates a surface TEM image obtained from a typical area of the pure DLC film, the image reveals that DLC film exhibits amorphous carbon structure, there are no distinguishable diffraction rings, which is a typical diamond-like structure. Figure 6(b) shows the TEM image with and corresponding selected area energy disperse spectroscopy (EDS) of the Cr-DLC film deposited at a sputtering current of 0.4 A. It is seen that the Cr-DLC film has nanocomposite structure in which Cr nanoparticles (the black dots in the TEM images) are uniformly embedded in amorphous carbon matrix. With combination of the following EDS of C (the red dots), Cr (the yellow dots) and XPS, we will then be able to know these nanoparticles are Cr compounds and elemental substances.

3.2 Mechanical Properties

Figure 7 shows the elastic modulus, nano-hardness, fracture toughness, and residual stress of the four films under different Cr target currents. The fracture toughness is determined by the elastic modulus and the nano-hardness and is greatly affected by the hardness of the film (Ref 42). The results show that the nano-hardness, elastic modulus, and fracture toughness of the film all increase first and then decrease with the increase of the Cr target current. During the deposition process, the particles strike on the surface of the substrate in a high-energy and high-speed under the action of the bias voltage and the ion source. The deposition of the new particles limits the diffusion behavior of the particles on the surface and causes compressive stress. The layered carbon structure is made up of sp^2 hybrid bonds and usually limited in space during the process of nucleation growth, it is forced to change to a higher coordination number. Particles with higher energy are more likely to break through the energy potential, bonding between atoms. Under the combined action of the two effects, the content of the sp^3 hybrid phase in the film structure gradually increases. The effect of sp^3 hybridization on the mechanical properties in the film is much larger than that of the sp^2 hybrid phase. The three-dimensional carbon structure of sp^3 is the result of the combination of covalent bonds in all directions, which is higher than the van der Waals bonding between the sp^2 interlayers. The hardness and shear strength of the films deposited at a sputtering current of 0.4 A are higher than the other samples, as shown in Fig. 7(a). At the same time, the Cr atoms in the deposition process bond with the C carbon atoms and O atoms, and the metal carbides and metal oxides are all hard particles that are uniformly distributed in carbon three-dimensional network structure during deposition process to bring the effect of dispersion strengthening, which can improve

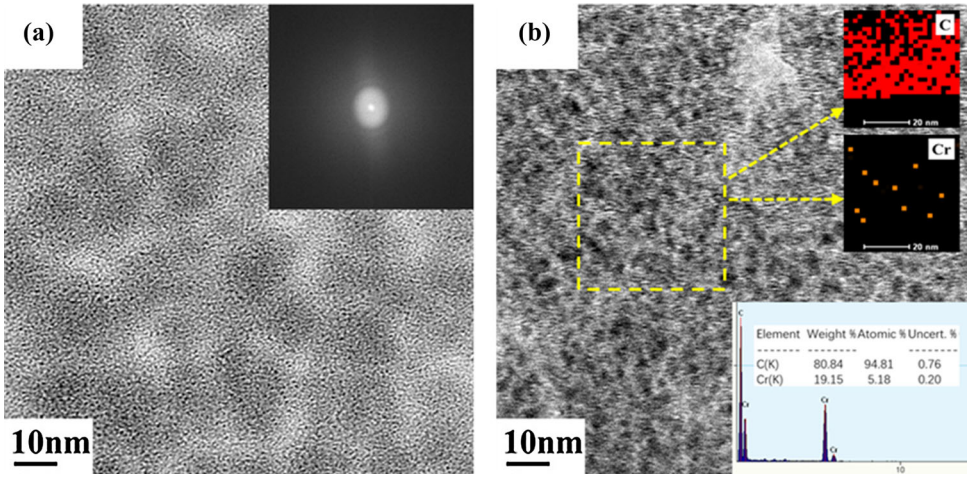

Fig. 6 (a) Typical TEM micrograph of the pure DLC, (b) TEM and corresponding EDS of the Cr-DLC film with the sputtering current at 0.4A

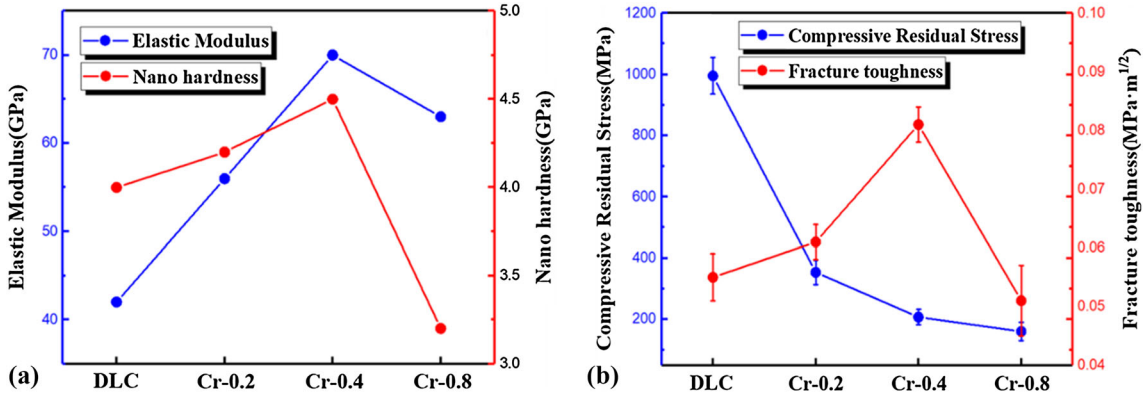

Fig. 7 (a) Elastic modulus and hardness of films, (b) Compressive residual stress and fracture toughness of films

the hardness and toughness of the film. However, when the current increased to 0.8 A, the Cr content in the film is around 22 at.%, which is twice as high as 0.4 A.

According to the XPS analysis, about half of the Cr in the film exist in formation of metal. Although the hardness of chromium carbide and oxide is high, Cr is a plastic metal and has a strong plastic deformation ability. In the case of a small amount of doping, metal Cr is embedded in the three-dimensional network of films with different size atomic clusters to improve the film's hardness and maintain the film's toughness. When the doping is in excess, the strong plasticity becomes dominant, the hardness and elastic modulus of the film are significantly reduced (Ref 43). During the whole doping process, both the elastic modulus and hardness increased first and then decreased. The proper content of Cr doping is a critical factor to ensure good mechanical properties by changing the structure of the film.

Figure 7(b) shows the relationship between the films' fracture toughness and internal stress. The fracture toughness is determined by the hardness and elastic modulus of the film. The change trend is consistent with the first two, and internal stress gradually decreases with the increase of doping content. The particles impact the surface of the substrate with high energy and high velocity and deposit on the surface, which cannot migrate because of high internal stress, which contributes to forming the sp^3 hybrid phase. However, both the sp^2 hybrid bonds and sp^3 hybrid bonds are classified as covalent bonds, and they can only form at specific positions in two or three dimensions. They are also easily squeezed cause the bond angle of the atom to be distorted during the bonding process, and the electron cloud stack to have a stronger bond strength than either the ionic bond or the metal bond. Therefore, the film exhibits a high internal stress when it is not doped. With the doping of Cr atoms, the C atoms are released from their typical state of being difficult to bond due to space limitations, preferentially forming C-Cr bonds. The formation of ionic bonds has no directional requirements (Ref 44, 45), which significantly reduces the stress generated by covalent bonds distortion. In addition, the strong plasticity of the elemental material shows a continuous trend of decreasing internal stress. The internal stress is reduced by more than 80% when the doping content is 22 at.%.

3.3 Tribological Properties

Figure 8 shows the friction coefficient and wear rate of the films. The film with Cr target currents of 0, 0.2 and 0.4 A were tested for a total of 20 min. After a short fluctuating stage, the friction coefficient keeps stable, except the sample prepared with a current of 0.8 A. The pure DLC film exhibits a low coefficient of friction, which is represented by a red curve in Fig. 8(a). Its average coefficient of friction is only 0.068, because the proportion of sp^2 hybrid bonds in pure DLC films is as high as 70%. The corresponding graphite phase has a strong self-lubricating property that allows interlayer slippage to occur easily under the action of shearing force, and the film is transferred to form a transfer film on the grinding pair (Ref 46). The friction coefficient fluctuation decreases during the stable phase, and although the hardness and toughness are lower, the self-lubricating property of graphite phase has a good lubricating effect under low contact stress. As shown in Fig. 9, the pure DLC film has the shallowest wear-scar depth and the wear rate is relatively low.

After doping the DLC film with Cr, only the film with a sputtering target current of 0.4 A did not fail within the friction test time, and the other two doped samples failed at different

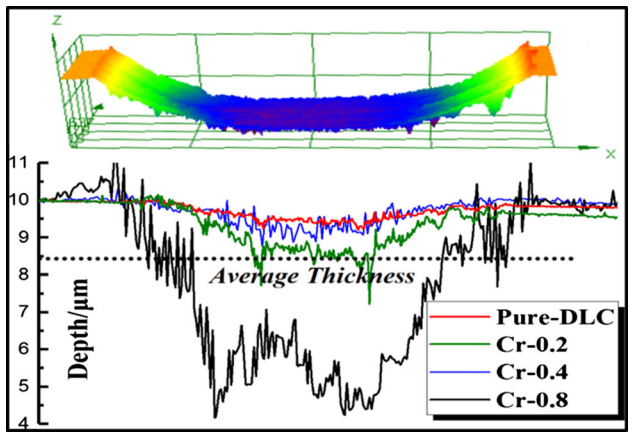

Fig. 9 Cross-sectional profiles of the wear track on DLC and Cr-DLC films

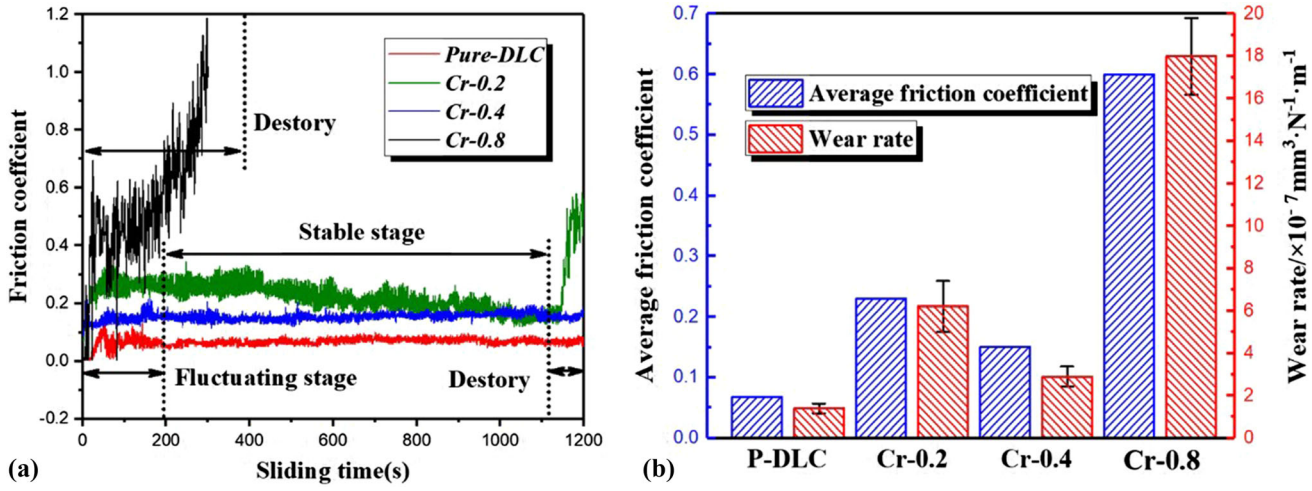

Fig. 8 (a) Friction coefficient curves; (b) Average friction coefficient and wear rate of DLC and Cr-DLC films

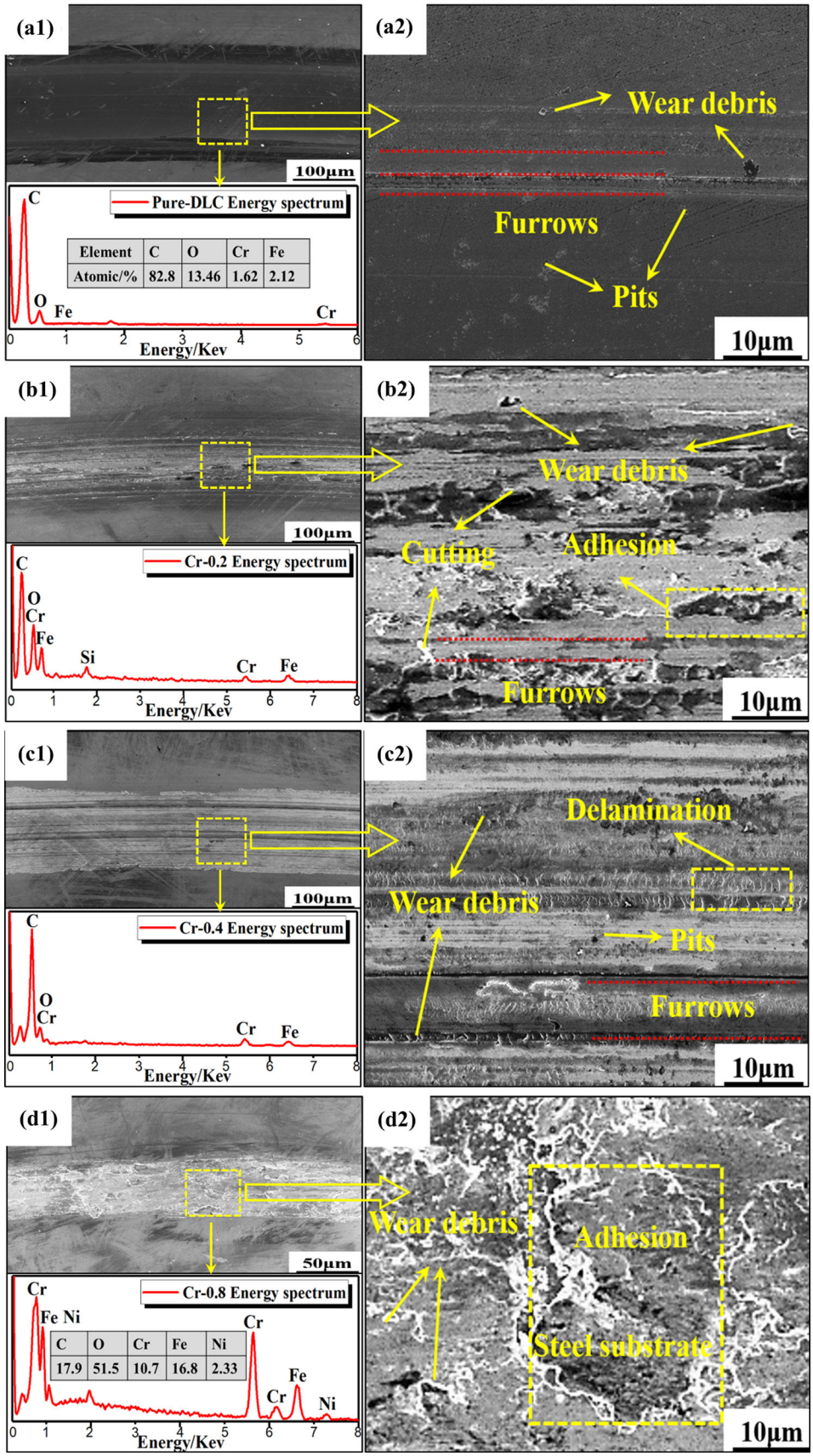

Fig. 10 Wear morphologies of the pure-DLC (a1, a2), Cr-0.2 (b1, b2), Cr-0.4 (c1, c2), and Cr-0.8 (d1, d2) films under atmospheric environment, and EDS of surface

stage. Metal doping changes the internal composition and structure of the film, especially the strong carbon metal, which has a more obvious influence on the three-dimensional network structure in the DLC film. After Cr doping, some of the carbon atoms are transformed from the layered graphite phase to the hard diamond phase, while others combine with the C and Cr atoms and become a hard metal carbide. Therefore, the self-lubricating property decreases remarkably, and the friction coefficient increases significantly. The film with a target current of 0.2 A most likely fails due to its poor mechanical properties during the test time. Hardness is an important factor for the wear resistance of the material. The film with a target current of 0.8 A failed immediately after a short fluctuating stage. It can be inferred that a large amount of metal doping lead to a significant decrease in the mechanical properties of the film, causing the film to fail as soon as it enters the stable stage. While continually increasing the target current, the COF decreases slightly. The films prepared with target current of 0.4 A demonstrated the best mechanical properties, showing great wear resistance and no failure occurred. And it can be clearly observed that the wear rate kept consistent with the average friction coefficients.

The tribological mechanism of the film after friction and wear was analyzed by SEM and energy dispersion spectroscopy (EDS). The results shown in Fig. 10(a-d) show the surface morphology and composition of pure DLC, 0.2, 0.4 and 0.8 A, respectively. As shown in Fig. 10(a1) and (a2), because of the good self-lubricity ability of the pure DLC film, the surface of the wear scar is relatively even and flat, wear form is mainly abrasive wear of the hard diamond phase, the wear degree is slight, and the wear-scar depth is about 0.5 μm that can be seen from Fig. 9. Analysis of wear-scar morphology shows that it consists of carbon and carbon oxides. The film with a target current of 0.2 A has an adhesive nature in a wide range wear because reduced graphite content leads to the decreasing of the mechanical properties. In Fig. 10(b1), (b2), (c1), and (c2), some of the adhesive products cover the surface of the furrow, but furrows can still be seen by hard carbides and oxides. The sharp object has the most obvious influence on the film during the friction and wear process. Hard particles of this size cause micro-cutting during the friction process and can remove a significant amount of material.

EDS results in Fig. 10(b1) show that the composition of the wear-scar contains Si and Fe, both of these being elements present in a stainless-steel substrate. From the green curve in Fig. 9, it can be seen that the depth of the partial wear-scar exceeded the average thickness of the film and failed, corresponding to the friction coefficient increasing suddenly in Fig. 8 at the end of the experiment. Compared with the film with a target current of 0.4 A in Fig. 10(c1) and (c2), obvious furrows and partial layered stack areas can be observed. Because of the higher toughness and hardness of the film, it has better wear resistance and no large-area adhesive wear or peeling behavior. The depth of the wear-scar measured during the test time was less than 1 μm and did not reach the average thickness of the film, so no failure behavior occurred. As shown in Fig. 10(d1) and (d2), the mechanical properties and tribological properties of the film at the maximum current are severely damaged because of over-doping. The depth of the wear scar is much larger than the average thickness of the film, and the grinding ball is in contact with the Si substrate directly, which has a low hardness and high plasticity, so a large area of adhesion on the surface and friction increases significantly.

4. Conclusions

The DLC films of various levels of Cr doping were prepared by unbalanced magnetron sputtering technique. The effects of Cr content on the microstructure, mechanical properties, and tribological properties of the films were investigated. The relevant results and conclusions can provide guidance on similar metal doping.

(1) Metal carbides, oxides, and elemental metal particles formed by Cr doping are uniformly distributed in the gaps of the three-dimensional network of the film to reduce surface roughness. High-energy and high-speed particles can increase the surface compressive stress significantly during the deposition process and promote the generation of sp^3 hybridization in the film, causing the increment of diamond phase in the film.
(2) Most of the Cr atoms still exist in the form of a simple metal. When the doping content is less than 15 at.%, the hard metal compounds occupy a predominant position, hardness and toughness are better than pure DLC films. As the doping content continues to increase, the soft metal elements occupy a predominant position, and the mechanical properties are severely degraded. Therefore, an appropriate amount of doping can improve the mechanical properties of the film effectively.
(3) After Cr doping, the self-lubricating property decreased, caused by the generation of sp^3 phase and the formation of hard carbides and oxides, making the friction coefficient increase. The form of wear is mainly abrasive, and the excessive plasticity of over-doping not only destroys the mechanical properties of the film but also significantly reduces the wear resistance properties of the film.

Acknowledgments

The authors acknowledge financial support by National Natural Science Foundation of China (51675531, 51535011, 51605451), the Pre-Research Program in National 13th Five-Year Plan (61409230603, 61409220205), and Joint Fund of Ministry of Education for Pre-research of Equipment for Young Personnel Project (6141A02033120).

References

1. X. Xu, J. Qin, and Z. Li, Research Advances of Graphene, *Prog. Chem.*, 2009, **21**(12), p 2559–2567
2. L. Bai, G. Zhang, Z. Lu, Z. Wu, Y. Wang, L. Wang, and P. Yan, Tribological Mechanism of Hydrogenated Amorphous Carbon Film Against Pairs: A Physical Description, *J. Appl. Phys.*, 2011, **110**(3), p 6140–6748
3. Ö.D. Coşkun and T. Zerrin, Optical, Structural and Bonding Properties of Diamond-Like Amorphous Carbon Films Deposited by DC Magnetron Sputtering, *Diam. Relat. Mater.*, 2015, **56**, p 29–35
4. P. Mahtani, K.R. Leong, I. Xiao, A. Chutinan, N.P. Kherani, and S. Zukotynski, Diamond-Like Carbon Based Low-Emissive Coatings, *Sol. Energy Mater. Sol. Cells*, 2011, **95**(7), p 1630–1637
5. S.C.H. Kwok, W. Zhang, G.J. Wan, D.R. McKenzie, M.M.M. Bilek, and P.K. Chu, Hemocompatibility and Anti-Bacterial Properties of Silver Doped Diamond-Like Carbon Prepared by Pulsed Filtered Cathodic Vacuum Arc Deposition, *Diam. Relat. Mater.*, 2007, **16**(4–7), p 1353–1360

6. D. Fu, D. Xie, C.H. Zhang, C. Zhang, and L. Liu, Preparation and Characteristics of Nanoscale Diamond-Like Carbon Films for Resistive Memory Applications, *Chin. Phys. Lett.*, 2010, **27**(9), p 225–228
7. B.Y. Zhang, Q.U. Yan-Qing, H.M. Xie, and C.Y. Nie, Review of Preparation and Application of Diamond-Like Carbon Films, *Surf. Technol.*, 2007, **36**(3), p 70–73
8. A.A. Voevodin, J.M. Schneider, C. Rebholz, and A. Matthews, Multilayer Composite Ceramicmetal-DLC Coatings for Sliding Wear Applications, *Tribol. Int.*, 1996, **29**(7), p 559–570
9. F.J. Li, S. Zhang, J. Kong, Y. Zhang, and W. Zhang, Multilayer DLC Coatings Via Alternating Bias During Magnetron Sputtering, *Thin Solid Films*, 2011, **519**(15), p 4910–4916
10. X. Sui, J. Liu, S. Zhang, J. Yang, and J. Hao, Microstructure, Mechanical and Tribological Characterization of CrN/DLC/Cr-DLC Multilayer Coating with Improved Adhesive Wear Resistance, *Appl. Surf. Sci.*, 2018, **439**, p 24–32
11. J.Y. Jao, S. Han, L.S. Chang, Y.-C. Chen, C.-L. Chang, and H.C. Shih, Formation and Characterization of DLC:Cr: Cu Multi-layers Coating Using Cathodic Arc Evaporation, *Diam. Relat. Mater.*, 2009, **18**(2–3), p 368–373
12. Y.J. Jo, T.F. Zhang, M.J. Son, and K.H. Kim, Synthesis and Electrochemical Properties of Ti-Doped DLC Films by a Hybrid PVD/PECVD Process, *Appl. Surf. Sci.*, 2018, **433**, p 1184–1191
13. M. Goto, Preparations and Tribological Properties of Soft-Metal/DLC Composite Coatings by RF Magnetron Sputter Using Composite Targets, *Int. J. Mech. Mater. Des.*, 2018, **14**(3), p 313–327
14. F.M. Wang, M.W. Chen, and Q.B. Lai, Metallic Contacts to Nitrogen and Boron Doped Diamond-Like Carbon Films, *Thin Solid Films*, 2010, **518**(12), p 3332–3336
15. S. Shen, J. Chen, X. Wang, L. Zhao, and L. Guo, Microwave-Assisted Hydrothermal Synthesis of Transition-Metal Doped ZnIn2S4 and Its Photocatalytic Activity for Hydrogen Evolution Under Visible Light, *J. Power Sour.*, 2011, **196**(23), p 10112–10119
16. R. Fernandes, N. Patel, A. Miotello, R. Jaiswal, and D.C. Kothari, Dehydrogenation of Ammonia Borane with Transition Metal-Doped Co-B Alloy Catalysts, *Int. J. Hydrog. Energy*, 2012, **37**(3), p 2397–2406
17. N. Boubiche, J. El Hamouchi, J. Hulik, M. Abdesslam, C. Speisser, F. Djeffal, and F. Le Normand, Kinetics of Graphitization of Thin Diamond-Like Carbon (DLC) Films Catalyzed by Transition Metal, *Diam. Relat. Mater.*, 2019, **91**, p 190–198
18. W. Dai and A. Wang, Synthesis, Characterization and Properties of the DLC Films with Low Cr Concentration Doping by a Hybrid Linear Ion Beam System, *Surf. Coat. Technol.*, 2011, **205**(8–9), p 2882–2886
19. L. Yang, A. Neville, A. Brown, P. Ransom, and A. Morina, Friction Reduction Mechanisms in Boundary Lubricated W-Doped DLC Coatings, *Tribol. Int.*, 2014, **70**, p 26–33
20. X.S. Tang, H.J. Wang, L. Feng, L.X. Shao, and C.W. Zou, Mo Doped DLC Nanocomposite Coatings with Improved Mechanical and Blood Compatibility Properties, *Appl. Surf. Sci.*, 2014, **311**, p 758–762
21. M. Masuko, T. Ono, S. Aoki, A. Suzuki, and H. Ito, Friction and Wear Characteristics of DLC Coatings with Different Hydrogen Content Lubricated with Several Mo-containing Compounds and Their Related Compounds, *Tribol. Int.*, 2015, **82**, p 350–357
22. J.F.R. Robertson, Diamond-Like Amorphous Carbon, *Mater. Sci. Eng. R Rep.*, 2002, **37**(4–6), p 129–281
23. C. Donnet and A. Erdemir, Historical Developments and New Trends in Tribological and Solid Lubricant Coatings, *Surf. Coat. Technol.*, 2004, **180-181**(3), p 76–84
24. K. Holmberg, H. Ronkainen, A. Laukkanen, and K. Wallin, Friction and Wear of Coated Surfaces-Scales, Modelling and Simulation of Tribomechanisms, *Surf. Coat. Technol.*, 2007, **202**(4), p 1034–1049
25. L. Bai, N. Srikanth, H. Wu, Y. Liu, B. Liu, and K. Zhou, Investigation on Tensile Behaviors of Diamond-Like Carbon Films, *J. Non-Cryst. Solids*, 2016, **443**, p 8–16
26. N. Dwivedi, S. Kumar, H.K. Malik, C. Sreekumar, S. Dayal, C.M.S. Rauthan, and O.S. Panwar, Investigation of Properties of Cu Containing DLC Films Produced by PECVD Process, *J. Phys. Chem. Solids*, 2012, **73**(2), p 308–316
27. F.R. Marciano, L.F. Bonetti, L.V. Santos, N.S. Da-Silva, E.J. Corat, and V.J. Trava-Airoldi, Antibacterial Activity of DLC and Ag-DLC Films Produced by PECVD Technique, *Diam. Relat. Mater.*, 2009, **18**(5-8), p 1010–1014
28. Y. Wu, J. Chen, H. Li, L. Ji, Y. Ye, and H. Zhou, Preparation and Properties of Ag/DLC Nanocomposite Films Fabricated by Unbalanced Magnetron Sputtering, *Appl. Surf. Sci.*, 2013, **284**(11), p 165–170
29. X. Yu, M. Hua, and C. Wang, Influence of Ag Content and Nanograin Size on Microstructure, Mechanical and Sliding Tribological Behaviors of Ag-DLC Films, *J. Nanosci. Nanotechnol.*, 2009, **9**(11), p 6366–6371
30. R. Paul, R. Bhar, and A.K. Pal, Field Emission Properties of Composite Nano-Au/DLC Films Prepared by CVD Technique, *Mater. Res. Bull.*, 2010, **45**(5), p 576–583
31. M. Guozheng, X. Binshi, W. Haidou, C. Shuying, and X. Zhiguo, Excellent Vacuum Tribological Properties of Pb/PbS Film Deposited by RF Magnetron Sputtering and Ion Sulfurizing, *ACS Appl. Mater. Interfaces.*, 2014, **6**(1), p 532–538
32. W. Zhai, N. Srikanth, L.B. Kong, and K. Zhou, Carbon Nanomaterials in Tribology, *Carbon*, 2017, **119**, p 150–171
33. J.A. Santiago, I. Fernández-Martínez, J.C. Sánchez-López, T.C. Rojas, A. Wennberg, V. Bellido-González, J.M. Molina-Aldareguia, M.A. Monclús, and R. González-Arrabal, Tribomechanical Properties of Hard Cr-Doped DLC Coatings Deposited by Low-Frequency HiPIMS, *Surf. Coat. Technol.*, 2020, **382**, p 124899. https://doi.org/10.1016/j.surfcoat.2019.124899
34. M. Yan, X. Wang, S. Zhang, S. Zhang, X. Sui, W. Li, J. Hao, and W. Liu, Friction and wear properties of GLC and DLC coatings under ionic liquid lubrication, *Tribol. Int.*, 2020, **143**, p 106067
35. J. Wu, G. Wu, X. Kou, Z. Lu, and G. Zhang, Tribological Properties of Amorphous Carbon in Hydrochloric Acid with ta-C Counterpart, *Surf. Coat. Technol.*, 2019, **380**, p 125004
36. L. Tang, J. Kang, P. He, S. Ding, S. Chen, M. Liu, Y. Xiong, G. Ma, and H. Wang, Effects of Spraying Conditions on the Microstructure and Properties of NiCrBSi Coatings Prepared by Internal Rotating Plasma Spraying, *Surf. Coat. Technol.*, 2019, **374**, p 625–633
37. L. Fayette, B. Marcus, and M. Mermoux, Local Order in CVD Diamond Films: Comparative Raman, x-ray-diffraction, and x-ray-absorption Near-Edge Studies, *Phys. Rev. B*, 1998, **57**, p 14123–14132
38. S. Neuville, Quantum Electronic Mechanisms of Atomic Rearrangements During Growth of Hard Carbon Films, *Surf. Coat. Technol.*, 2011, **206**(4), p 703–726
39. K.K. Mishra, R. Rani, N. Kumar, T.R. Ravindran, K.J. Sankaran, and I.N. Lin, High Pressure Raman Spectroscopic Studies on Ultrananocrystalline Diamond Thin Films: Anharmonicity and Thermal Properties of the Grain Boundary, *Diam. Relat. Mater.*, 2017, **80**, p 45–53
40. A. Ferrari, Carlo, Determination of Bonding in Diamond-Like Carbon by Raman Spectroscopy, *Diam. Relat. Mater.*, 2002, **11**(3–6), p 1053–1061
41. A.C. Ferrari, B. Kleinsorge, N.A. Morrison, A. Hart, V. Stolojan, and J. Robertson, Stress Reduction and Bond Stability During Thermal Annealing of Tetrahedral Amorphous Carbon, *J. Appl. Phys.*, 1999, **85**(10), p 7190–7191
42. L. Tang, P. He, J. Kang, L. Wang, S. Ding, S. Chen, X. Zhu, F. Xie, L. Zhou, G. Ma, and H. Wang, Significantly Enhanced Mechanical and Tribological Properties of Co-Based Alloy Coatings by Annealing Treatment, *Tribol. Int.*, 2020, **146**, p 106265. https://doi.org/10.1016/j.triboint.2020.106265
43. C. Zou, H.J. Wang, L. Feng, and S.W. Xue, Effects of Cr Concentrations on the Microstructure, Hardness, and Temperature-Dependent Tribological Properties of Cr-DLC Coatings, *Appl. Surf. Sci.*, 2013, **286**, p 137–141
44. J.H. Choi, H.S. Ahn, S.C. Lee, and K.R. Lee, Stress Reduction Behavior in Metal-Incorporated Amorphous Carbon Films: First-Principles Approach, *J. Phys: Conf. Ser.*, 2006, **29**, p 155–158
45. C. Casiraghi, A.C. Ferrari, R. Ohr, A.J. Flewitt, and J. Robertson, Dynamic Roughening of Tetrahedral Amorphous Carbon, *Phys. Rev. Lett.*, 2003, **91**(22), p 226104
46. Z. Piao, Z. Zhou, J. Xu, and H. Wang, Use of x-ray Computed Tomography to Investigate Rolling Contact Cracks in Plasma Sprayed Fe-Cr-B-Si Coating, *Tribol. Lett.*, 2018, **67**(1), p 11